The Gas Phase Anisole Dimer: A Combined High-Resolution Spectroscopy and Computational Study of a Stacked Molecular System†

G. Pietraperzia,*,‡,§ M. Pasquini,§ N. Schiccheri,‡ G. Piani,‡ M. Becucci,‡,§ E. Castellucci,‡,§ M. Biczysko,*,∥ J. Bloino,∥,⊥ and V. Barone⊥

LENS, Polo Scientifico e Tecnologico dell'Università di Firenze, Via Nello Carrara 1, 50019 Sesto Fiorentino (FI), Italy, Dipartimento di Chimica, Polo Scientifico e Tecnologico dell'Università di Firenze, Via della Lastruccia 3, 50019 Sesto Fiorentino (FI), Italy, Dipartimento di Chimica, Università Federico II, Complesso Universitario Monte S.Angelo, via Cintia, 80126 Napoli, Italy, Scuola Normale Superiore, Piazza dei Cavalieri 7, 56126 Pisa, Italy, and Istituto per i Processi Chimico Fisici, Area della Ricerca-CNR, via G. Moruzzi, 56124 Pisa, Italy

Received: April 8, 2009; Revised Manuscript Received: September 18, 2009

The gas phase structures of anisole dimer in the ground and first singlet electronic excited states have been characterized by a combined experimental and computational study. The dimer, formed in a molecular beam, has been studied by resonance-enhanced multiphoton ionization and high-resolution laser-induced fluorescence techniques. The assignment of the rotational fine structure of the $S_1 \leftarrow S_0$ electronic transition origin has provided important structural information on the parallel orientation of aromatic rings of anisole moieties. By comparison with the DFT/TD-DFT computational results, it has been possible to infer the detailed equilibrium structure of the complex. The analysis of the equilibrium structure and interaction energy confirms that the anisole dimer is stabilized by dispersive interaction in the gas phase. This is, to the best of our knowledge, the first detailed work (reporting both theoretical and high-resolution experimental data) on an isolated cluster in the π-stacking configuration.

Introduction

Properties of complex systems are determined by cumulative effect of many competing processes involving different parts of the same molecule and/or surrounding ones. Attractive interaction between π-electron systems is one of the main noncovalent forces governing molecular recognition and influencing protein structures, DNA, and self-assembled supramolecular architectures.[1] Usually we refer to stacking interaction in all cases where two aromatic rings are placed on parallel planes at a distance of 3.4−4 Å, allowing a weak interaction between the two, at least partially overlapped, rings. To study the details of the interaction of two aromatic molecules in this spatial arrangement, it is necessary to isolate them from any possible external perturbation. This is possible in the molecular beam experiments, and for this reason many biological model systems have been recently investigated with gas phase spectroscopic techniques.[2] The very accurate data from high-resolution spectroscopy in a molecular beam allow for the description of the equilibrium structure with great detail. Unfortunately, only a limited set of parameters can be experimentally determined. Sometimes it is possible to increase the information by using isotopic substitution methods, through the rotational constants. However, approximations and modeling are always needed dealing with large size species. It needs to be stressed that when both interacting molecules are of similar size, the simplified description in which a structured molecule is interacting with a sphere is not feasible, in variance to the systems in which an aromatic molecule is interacting with a rare gas atom or with small inorganic molecules like water and ammonia. Moreover, the building of appropriate models is not trivial especially if weak interaction forces are dominating.[3–10]

It should be noted that the correct description of the $\pi-\pi$ interactions is a challenging task for computational chemistry. The Hartree−Fock molecular orbital theory describes each electron in the average field of the other electrons, and so it is unable to describe the instantaneous fluctuations giving rise to dispersion forces. Also the standard density functional theory essentially relies on local approximations for the density, and so it is incapable of accurately describing the dispersion forces. Wave functions based correlation methods (such as Møller-Plesset perturbation theory, Coupled Cluster methods) with extended basis sets are required for a qualitatively accurate description of the benzene dimer.[11] However, it is not yet feasible to explore the potential energy surface (PES) for complexes of a similar size by means of these highly accurate ab initio approaches. Thus, to fully account for all possible inter- and intramolecular interactions, in particular to correctly describe stacking or long-range dispersion/van der Waals interactions, it is necessary to make use of the recent developments in the DFT theory.[12–16]

Despite the great effort dedicated to spectroscopic studies of bimolecular complexes formed by aromatic molecules in the gas phase, only few of them have been studied under high-resolution conditions. In particular, the cases of phenol dimer[4] and benzene dimer[11,17] are relevant with respect to the present study.

The benzene dimer can be considered as the simplest prototype system of $\pi-\pi$ interactions; unfortunately, the small

† Part of the "Vincenzo Aquilanti Festschrift".

* Corresponding authors, gianni.pietraperzia@unifi.it and malgorzata.biczysko@unina.it.

‡ LENS, Polo Scientifico e Tecnologico dell'Università di Firenze.

§ Dipartimento di Chimica, Polo Scientifico e Tecnologico dell'Università di Firenze.

∥ Dipartimento di Chimica, Università Federico II.

⊥ Scuola Normale Superiore and Istituto per i Processi Chimico Fisici, Area della Ricerca-CNR.

10.1021/jp903236z
Published on Web 10/08/2009

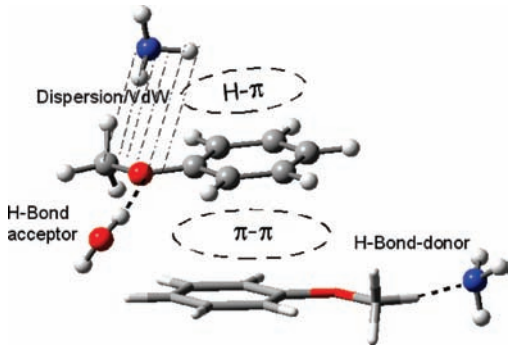

Figure 1. Different possible interactions in complexes of anisole.

binding energy (~2−3 kcal mol^{-1}) in the gas phase makes it a challenge for both experimental and theoretical studies. The dimer is stable only at low temperatures and is typically prepared in supersonic jet expansions. The different experimental techniques employed to date have provided seemingly contradictory results and are only consistent if the complex is really weakly bound and at least two different potential energy minima exist or if the system is highly fluxional with low barriers. Experimental[17] and theoretical[11,18] works suggest that the most favorable configurations are the perpendicular T-shaped and parallel-displaced geometries, but only the former has been clearly observed in a microwave experiment.[17] The eclipsed sandwich configuration has been predicted to lay somewhat higher in energy. From the theoretical point of view the binding energy of the dimer is primarily due to London dispersion interactions,[18] derived from favorable instantaneous-multipole/induced-multipole charge fluctuations.

The phenol molecule, one of the simplest substituted benzenes, is not an ideal choice for studies of the weakest intermolecular interactions due to its capability to form strong hydrogen bonds. Several gas phase complexes containing phenol have been investigated experimentally,[19,20] and in all the reported cases the leading interaction has been unambiguously assigned as the formation of a hydrogen bond. Also in phenol dimer, the hydrogen bond is the leading interaction, with one of the molecules acting as an acid and the other as a base. Such a structure is clearly evidenced by the presence of two systems of bands related to the original $S_1 \leftarrow S_0$ electronic transition in the two units. Nevertheless, in phenol dimer the aromatic rings are more tilted than it should be expected for a pure trans-linear arrangement, as observed, e.g., for the phenol−water cluster. This deviation should be a consequence of the additional dispersive interactions between the two aromatic rings.

We decided to study the properties of anisole dimer. With respect to the phenol dimer the change of the −OH functional group with a $-OCH_3$ group makes impossible the formation of the strong intermolecular hydrogen bond. Anisole is particularly interesting thanks to the coexistence of prototypical functional groups: the aromatic electron system, the electron lone pair on the oxygen atom, H-atoms both on the ring and on the methyl group. As a result, anisole can be involved in a number of different interactions (see Figure 1): hydrogen bonding, van der Waals forces, dipole−dipole interactions. Moreover, in many cases none of these mechanisms is clearly dominant and a delicate balance of different terms is likely to be expected. Recent studies of the anisole−water[8,9] and anisole−ammonia[10,21] adducts highlighted the complexity of the potential energy surface of molecular systems that involve the anisole. For the anisole−water complex,[8,9,22] a hydrogen bond (OH···O) is formed with the oxygen of anisole leading to a planar structure. For the anisole−NH_3 adduct a nonplanar geometry[10,21] is determined by the interactions between ammonia and the delocalized π-electron density from the anisole ring.

We are reporting here a study on the anisole dimer, a system for which hypotheses on the equilibrium structure cannot be suggested by chemical intuition only and the complexity of the potential energy surface (PES) requires a systematic approach. A good compromise between physical reliability and computational speed is certainly given by classical molecular mechanics (MM) methods. Standard MM techniques, combined with empirical force fields, have been used in recent literature to study interactions between aromatic systems.[23−26] MM represents in our study only a preliminary phase that should provide a set of possible and reliable candidate structures, which will be further refined at the ab initio level. It has been shown that for the anisole−ammonia and anisole−water complexes[12] DFT approaches with semiempirical correction for dispersion (DFT-D),[13,14] a recently parametrized semilocal density-functional (M05-2X)[15] and the long-range correction scheme included in the LC-ωPBE model,[16] provide reliable geometrical structures both in ground and in excited states. Thus these same functionals have been also applied in the present study.

In our study experimental and computational approaches have been necessarily combined in order to determine the ground and excited state geometry structure of the anisole dimer. It should be anticipated that in this complex the main stabilizing interaction is of dispersion type, and so it is the first clear example of a detailed study of a dimer exhibiting stacking interaction as a fundamental stabilization term.

As usual, unless otherwise specified, all along this paper we refer to anisole and anisole dimer as the species with the most abundant isotopic distribution, $C_6H_5-CH_3$ and $(C_6H_5-CH_3)_2$, respectively.

Experimental Section

The resonance enhanced multiphoton ionization (REMPI) and the high-resolution laser-induced fluorescence (HR-LIF) molecular beam spectrometers are described elsewhere.[8,27] Here we are reporting only some details relevant for the experiments. Anisole (both standard and with full H/D substitution on the methyl group) has been purchased from Aldrich and used without purification.

REMPI Experiment. The expanding gas mixture is produced flowing helium above the anisole sample, maintained at a temperature of −20 °C to lower its vapor pressure. In such a way a good quality of the spectrum can be assured: when the anisole concentration is too large, higher order clusters formation leads to a very broad, unstructured, band which can conceal the sharp signals of the dimer. The supersonic expansion is produced using a 500 μm diameter pulsed nozzle. The stagnation pressure is 300 kPa. The pressure in the expansion chamber is about 10^{-5} mbar when the pulsed valve is operating. In the time-of-flight mass spectrometer, differential pumping maintains the pressure in the 10^{-7} mbar scale. The radiation used for the REMPI experiment is generated by a frequency doubled dye laser operating on Coumarine 153A, pumped at 355 nm by a pulsed Nd:YAG laser, with a 10 Hz repetition rate. The nozzle opening is carefully synchronized with the laser pulses in order to maximize the dimer signal. The variable gain scheme was applied for an improved measurement of the anisole dimer spectrum.[28]

HR-LIF Experiment. In the HR-LIF experiment the anisole sample is placed inside the molecular beam source and the source is maintained at room temperature. Nozzle diameter is

100 μm, and the stagnation pressure is 300 kPa. It results in a 10^{-4} mbar pressure in the expansion chamber and 10^{-6} mbar in the interaction chamber. The laser system is formed by a single mode, frequency stabilized ring dye laser, operating with Rhodamine 110, pumped by 9 W of laser radiation at 515 nm. The emission of the ring dye laser is sent to an external resonating cavity in which we generate the UV radiation. We are able to obtain up to 20 mW of 2 MHz line-width UV radiation. The fluorescence radiation emitted by the absorbing species is collected with a system of spherical mirror and lenses, and focalized on a photomultiplier tube where it is measured in photon counting regime. In the HR experiment it is extremely important to have spectra with an accurate frequency scale. We use one external, hermetically sealed, and temperature stabilized étalon as a frequency marker to monitor the fundamental frequency of the laser. We use this étalon in a scanning (spectrum analyzer) mode to collect information for each data point.[27] The exact free spectral range of the interferometer is determined by the combination differences method applied to the HR spectrum of the corresponding band of the anisole monomer and relying on microwave data.[29]

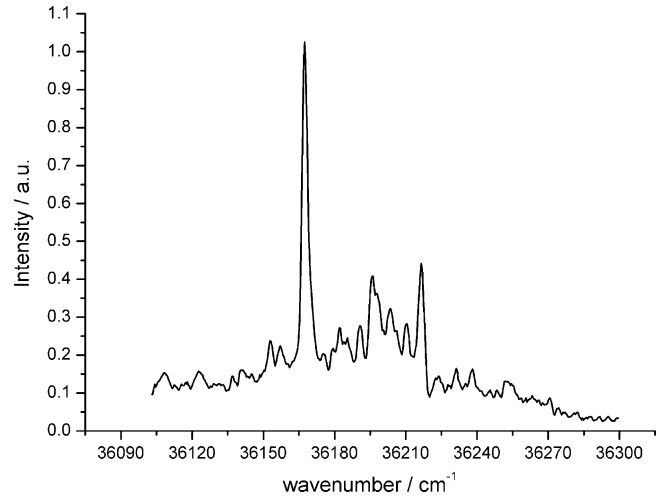

Figure 2. A portion of the REMPI spectrum around the origin band of the anisole dimer. The strongest band is assigned as the origin band, while the weaker bands are assigned to intermolecular vibrations in the molecular complex.

Computational Details

On the basis of a well-established procedure,[30–35] from a molecular dynamics simulation of the dimer in the NVT (constant number of particles, volume, and temperature) thermodynamical ensemble it was possible to determine all possible minima in the intermolecular PES of the anisole dimer by quenching about 3500 structures regularly sampled. The temperature was set to 300 K and the simulation box was a 25 Å side cube. The temperature is sufficient to guarantee breaking and re-forming of the complex several times during the simulation; the box is large enough to allow for the complete separation of the two units. The evolution of the system was calculated at 1 fs time resolution, and the configuration sampling was occurring with a 5 ps period. The anisole molecules have been modeled by the AMBER force field.[36] The atomic point charges (available upon request) have been obtained by a fit of the electrostatic potential obtained by B3LYP/6-31G(d,p) calculation. The conjugate gradient method has been used for minimization.

Geometry optimizations, at B3LYP-D[13,14] and MP2[37] levels with 6-31+G(d,p) basis set, have been carried out to initially distinguish local minima on the ground potential energy surface of anisole dimer starting from the set of eight representative configurations generated by MM. In such a way four distinct structures have been identified and subsequently refined by a counterpoise corrected optimization[38] at the MP2 level to avoid the basis-set superposition error (BSSE)[39] artifacts. From this set, three structures of similar stability have been chosen for further studies of anisole dimer in its ground and excited states by density functional theory (DFT) and its time-dependent extension (TD-DFT).[40] For DFT computations, approaches able to account for the dispersion/long-range interactions (B3LYP-D,[13,14] M05-2X,[15] and LC-ωPBE[16]) have been applied, but also the standard B3LYP[41] functional has been tested. It has been shown that double and triple-ζ quality basis sets with polarized functions on all atoms and diffuse functions on the heavy ones, for the anisole/water 1:1 complex,[9] are sufficient for obtaining qualitatively correct geometrical parameters. Therefore, having in mind the feasibility of excited state computations for the anisole dimer, the 6-31+G(d,p) basis set has been employed in all calculations. Zero-point vibrational energies, and the nature of the stationary points, have been evaluated by computing harmonic vibrational frequencies on the optimized structures. For the first singlet S_1 excited state vertical excitation energies, excited-state geometry optimization, and harmonic frequency calculations have been carried out at the TD-DFT[40] level. In the case of the excited state, interaction energies and BSSE corrections have been computed assuming the excitation to be localized on one of the anisole moieties, in particular the CP corrected binding energies have been calculated according to the scheme

$$\Delta E_{CP}^{*}(\mathrm{AB}) = [E_{\mathrm{AB}}^{\mathrm{AB}}(\mathrm{AB})^{*} - E_{\mathrm{A}}^{\mathrm{A}}(\mathrm{A})^{*} - E_{\mathrm{B}}^{\mathrm{B}}(\mathrm{B})] + [E_{\mathrm{AB}}^{\mathrm{A}}(\mathrm{A})^{*} + E_{\mathrm{AB}}^{\mathrm{B}}(\mathrm{B}) - E_{\mathrm{AB}}^{\mathrm{AB}}(\mathrm{A})^{*} - E_{\mathrm{AB}}^{\mathrm{AB}}(\mathrm{B})] \quad (1)$$

where $E_X^Y(Z)$ is the energy of subsystem Z at geometry X with basis set Y, A and B correspond to anisole excited (A) and spectrator (B) moieties, respectively, and excited state calculations are labeled by the asterisk (*). All these computations have been performed with a locally modified version of the Gaussian suite of programs for quantum chemistry.[14,42]

For the ground state, the energetics of the three local minima has been refined by single-point energy calculations at the coupled cluster level of theory including single and double excitations (CCSD),[43] with the cc-pVDZ (VDZ)[44] basis set. The CCSD energies have been corrected for the BSSE as evaluated at the MP2 level. The interaction energy has been also calculated by means of the symmetry-adapted intermolecular perturbation theory (SAPT)[45] and subsequently decomposed into individual first- and second-order interaction terms: electrostatic $E_{\mathrm{pol}}^{(1)}$, induction $E_{\mathrm{ind}}^{(2)}$, and dispersion $E_{\mathrm{disp}}^{(2)}$, accompanied by their respective exchange counterparts $E_{\mathrm{exch}}^{(1)}$, $E_{\mathrm{exch\text{-}ind}}^{(2)}$, and $E_{\mathrm{exch\text{-}disp}}^{(2)}$, as implemented in MOLPRO.[46]

Results and Discussion

Experimental REMPI and HR-LIF Data. The $S_1 \leftarrow S_0$ electronic transition of the anisole dimers was detected in a spectral region slightly red-shifted with respect to the corresponding transition of the bare anisole in a REMPI experiment as reported in Figure 2. The strongest band at 36167 cm^{-1} was assigned as the origin band of the $S_1 \leftarrow S_0$ electronic transition of the lightest anisole dimer (corresponding to a red shift of 217 cm^{-1} upon complex formation), the high-resolution spec-

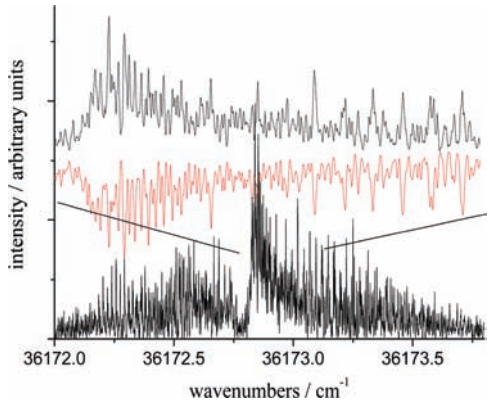

Figure 3. HR-LIF spectrum of the origin band of the $S_1 \leftarrow S_0$ electronic transition of the anisole dimer $(C_6H_5O-CD_3)_2$. The upper traces show an expansion of a portion of the spectrum to show the very good agreement between the experimental spectrum (upper trace) and the best simulation (central inverted trace).

trum of the same transition has been measured. We have studied also the corresponding bands of the anisole dimers formed by molecules deuterated at the methyl group (C_6H_5O-CD_3), in the two possible combinations: $(C_6H_5O-CD_3)_2$ and $(C_6H_5O-CH_3)-(C_6H_5O$-$CD_3)$. At a first glance, spectra obtained for the isotopically modified complexes show the same general features as for the lightest dimers. The HR spectrum of the origin band of the $S_1 \leftarrow S_0$ electronic transition of the $(C_6H_5O-CD_3)_2$ complex is reported in Figure 3.

In the case of anisole dimer the assignment of the rovibronic lines in high-resolution spectroscopy experiments is complicated by the relatively high dimension of the complex that leads to low values of the rotational constants. Difficulties in appropriate interpretation of experimental results are particularly enhanced for very congested spectra. To avoid the congestion of the spectrum, we chose a stagnation pressure of the helium gas that is high enough for a good cooling but not too high, to avoid substantial formation of large clusters.

The analysis of the rovibronic spectrum is further complicated by the lack of reliable hypotheses on the structure of the complex, but the results from QM calculations are a viable starting point. We have chosen a line by line assignment strategy, performed with the JB95 program[47] and using a rigid rotor Hamiltonian. It is worth mentioning that, in our usual experimental conditions, the rotational temperature of the molecules in the molecular beam is of the order of 4 K. In the current case (low values of the rotational constants) this leads, in the 2 cm^{-1} energy range of the experimental spectra, to about 8000 lines with intensity at least 0.5% of the strongest transition. Then, almost every line appearing in the spectrum is related to more than one rovibronic transition; thus particular care has to be exerted in the assignment of the spectrum. For the reasons mentioned above, several spectra simulations considering different equilibrium structures obtained from QM computations have been performed. Strong similarities between the experimental spectrum and the one simulated for the computed stacked structure appeared immediately evident. As an input for the assignment procedure, we have used the calculated rotational constants and band type. Then while the rotational constants have been fitted to best reproduce the experimental spectra, the band type was fixed to the theoretical values. The fitting procedure was performed by a line by line assignment starting from the most pronounced spectral features related to the strong lines present in the R branch. An iterative strategy of subsequent fittings and simulations allowed for a safe assignment of more than 500 single eigenstate transitions in the rovibronic spectrum. We have decided to limit the assignment to the most pronounced features, by looking only at experimental spectral lines with the intensity higher than 1% of the strongest transition and at single simulated lines that are stronger than 1% of the most intense one. No further improvement of the transition dipole moment was possible even after this analysis of the spectrum. From the experimental point of view, we have to stress that our data are mostly affected by errors on the intensity scale rather than on the frequency scale. Moreover, experimental spectra show a very complex pattern. These reasons precluded further refinement of the transition dipole moment values on the basis of the experimental results. The overall quality of the spectrum resulting from our fit has been checked by the calculation of the cross correlation of the experimental and the best simulated spectrum. Such strategy has been applied to all three isotopically different complexes, and in all cases cross-correlation between the experimental and simulated spectra higher than 95% of the experimental spectra autocorrelation value has been obtained. On the basis of such a good agreement, we are very confident of the overall quality of the fits. The comparison between experimental and simulated spectra for $(C_6H_5O-CD_3)_2$ is reported in Figure 3, while data relative to the fitting of spectra for the different isotopic species are listed in Table 1. The transition dipole moments reported in Table 1 derive from theoretical calculations. The projection of the transition dipole moments of the complexes on the principal inertia axis of the single anisole molecule suggests that the electronic transition of the complex corresponds, within a very good approximation, to a local excitation in a single anisole unit. In Figure 4 are reported the principal inertia axes and the dipole transition moments shown as a vector, either for the anisole dimer or for the anisole monomer. From the figure it is evident how the orientation of the calculated dipole transition moment for the two systems are essentially parallel with one another, with respect to the anisole units.

TABLE 1: Data Obtained from the Fitting Procedure of the Experimental High-Resolution Spectrum of the Origin Band of the Anisole Dimer[a]

	CH_3-CH_3	CH_3-CD_3	CD_3-CD_3
band center (cm^{-1})	36167.48	36170.16	36172.84
A″ (MHz)	841.19(3)	807.04(3)	773.22(2)
B″ (MHz)	390.24(3)	388.17(3)	385.53(3)
C″ (MHz)	325.27(3)	320.45(4)	314.81(3)
A′ (MHz)	834.26(3)	800.63(3)	767.20(2)
B′ (MHz)	396.51(3)	394.53(3)	391.65(3)
C′ (MHz)	332.56(3)	327.40(4)	321.41(5)
T (K)	4	4	4
% A	23.5	22.8	23.5
% B	2.3	3.6	1.2
% C	74.2	73.6	75.3
no. of assignments	517	452	481
σ (MHz)	8	7	6
Lorentzian (MHz)	20	20	20
Gaussian (MHz)	20	20	20

[a] The labeling of the columns is as follows: $CH_3 = C_6H_5O-CH_3$, $CD_3 = C_6H_5O-CD_3$. The number in parentheses represents the error expressed in units of the last digit, σ is the global standard deviation of the fit, and Lorentzian and Gaussian are the contributions to the linewidth used for the fitting and simulation procedure. The percentages of the A, B, and C type bands are taken from the DFT data.

Assessment of Computational Models. As mentioned in the Introduction, computational studies are necessary to assist determination of equilibrium structure for molecular aggregates

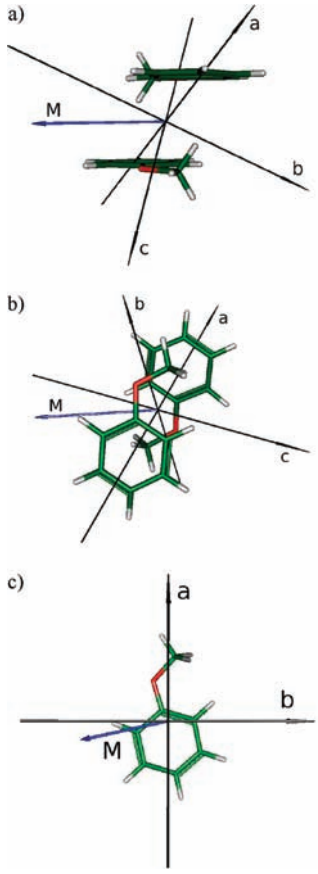

Figure 4. Calculated dipole transition moment (M) for the anisole dimer (viewed from two different sides (a) and (b) and of the anisole monomer (c). The dipole transition moment for the anisole molecule is contained in the anisole aromatic plane. The principal inertia axes are also reported. The dipole transition moment is an oscillating vector, and so the direction is chosen only for convenience.

with several possible interaction schemes. The current case is particularly challenging as dispersion forces need to be properly taken into account. Despite significant development of DFT methodologies able to describe dispersion interaction, their performance, in particular for the prediction of structures of weakly bounded complexes in excited electronic states, is not yet unequivocally established. In this context present work provides important benchmarking information by comparison with experimental data from high-resolution studies. From available methodologies B3LYP-D,[13,14] a recently parametrized semilocal density-functional (M05-2X[15]) and the long-range correction scheme included in the LC-ωPBE model,[16] has been chosen for further testing as it is shown to provide reliable geometrical structures both in the ground and in excited states for anisole complexes with water[9,12] and ammonia.[10,12] Results from DFT studies in the ground state have been also compared with standard ab initio methodologies accounting for the dispersion interaction, namely, MP2 and CCSD. It should be noted that the use of small basis sets combined with correlated QM computations can lead to a relatively large basis set superposition errors, so for MP2 and CCSD we refer to the counterpoise corrected (CP) values. For DFT approaches it has been checked that CP-corrected and uncorrected relative energies vary negligibly (within 0.1 kJ mol^{-1}).

The accuracy of DFT approaches has been evaluated comparing four structures corresponding to local minima on the ground potential energy surface, which are shown in Figure 5, and their relative energies listed in Table 2. In fact comparison of post-

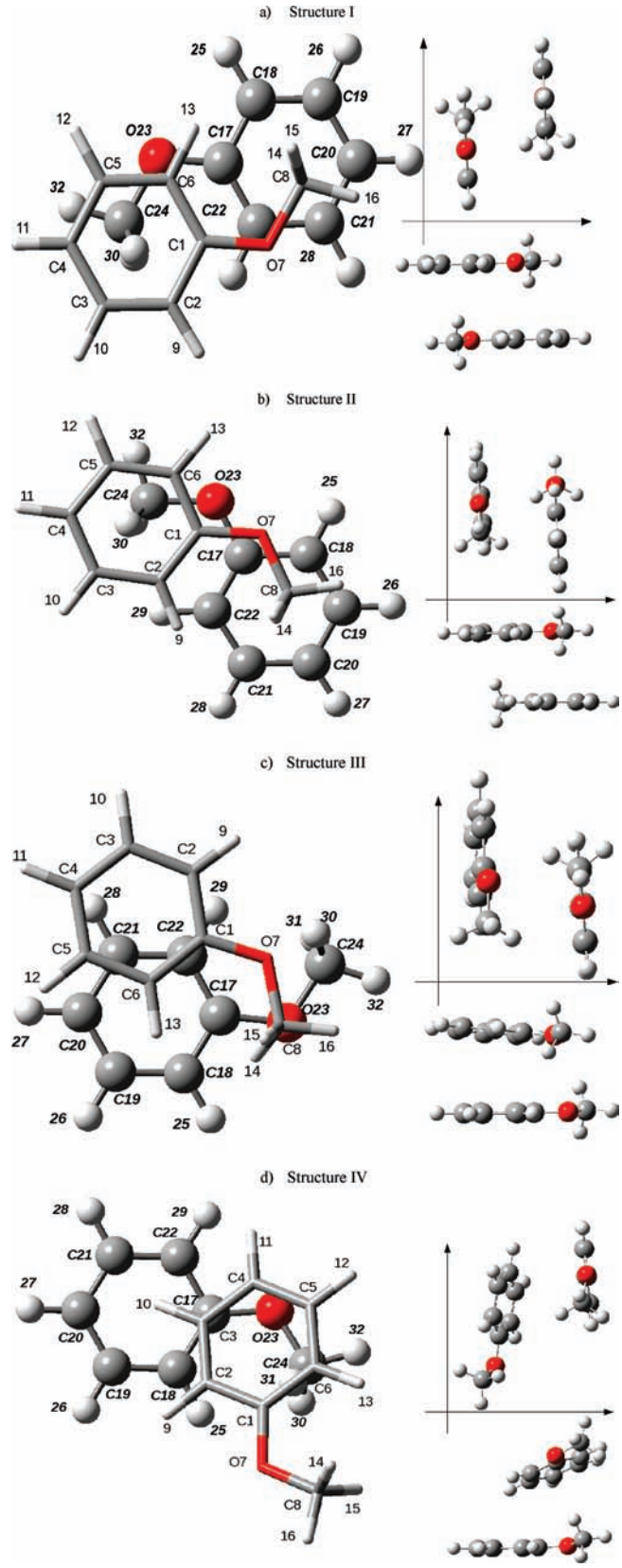

Figure 5. Geometry and atom numbering of four local minima structures of anisole dimer.

Hartree−Fock and DFT energies shows a very good agreement between the most accurate CCSD counterpoise corrected values and the LC-ωPBE and M05-2X results computed with a small basis set. Such good agreement supports the reliability of TD-DFT energies computed with the same basis set. It is apparent

TABLE 2: Relative Energies of Local Minima of Anisole Dimer in Its Ground and First Excited Electronic States[c]

	S_0								S_1	
	B3LYP	MP2	$MP2_{CP}$	B3LYP-D	LC-ωPBE	M05-2X	CCSD[a]	$CCSD_{CP}$[a,b]	TD-LC-ωPBE	TD-M05-2X
I	0	0	0	0	0	0	0	0	0	0
II	0.5	−0.3	1.0	0.9	1.2	1.6	0.7	0.9	1.0	0.8
III	−0.5	−4.1	−0.4	4.3	2.3	2.9	1.1	2.2	0.1	−0.2
IV	2.2	10.6	6.3	11.9	7.9					

[a] Computed for geometry optimized at the M05−2X/6-31+G(d,p) level. [b] BSSE correction computed at the MP2/cc-pVDZ level. [c] The 6-31+G(d,p) basis set has been used for DFT and MP2 calculations and cc-pVDZ for CCSD ones. All values in kJ/mol.

TABLE 3: Rotational Constants (in MHz) for Structures I−IV of Anisole Dimer in Its Ground State, Computed at Different Levels of Theory[a]

		B3LYP	MP2	$MP2_{CP}$	B3LYP-D	LC-ωPBE	M05-2X
I	A	822.82	856.52	822.2	886.46	877.02	856.95
	B	295.46	408.4	387.82	397.24	393.08	389.44
	C	252.98	339.83	321.08	336.35	330.57	325.73
	MAE (%)	16.2	3.7	1.4	3.5	2.2	0.7
II	A	810.77	901.59	848.4	903.82	885.95	883.11
	B	268.97	389.92	375.31	385.1	378.69	374.55
	C	262.11	359.19	339.46	356.4	346.73	343.66
	MAE (%)	18.0	5.9	3.0	6.1	4.9	4.9
III	A	828.88	712.73	679.75	695.9	839.31	814.81
	B	264.08	502.83	476.64	497.1	360.63	363.22
	C	236.87	395.75	371.11	386.7	311.79	313.07
	MAE (%)	20.3	21.9	18.4	21.1	4.0	4.6
IV	A	996.19	920.77	905.58	978.79		
	B	194.08	311.52	293.09	298.22		
	C	182.02	295.58	277.54	280.76		
	MAE (%)	37.6	13.0	15.8	17.9		

[a] The mean absolute error MAE (%) to the observed values is also reported.

that all methods predict structure IV as the least stable (we should also anticipate that its rotational constants, reported in Table 3, show the largest deviation from the experimental ones). For these reasons structure IV has been excluded from further analysis. Additional insights on the accuracy of tested DFT models may come from comparison with experimental data. In this case a good agreement between computed and experimental rotational constants indicates the most accurate computational model and, on the other hand, confirms experimentally observed structure of the complex. The ground state rotational constants (listed in Table 3) show that the smallest mean absolute error (MAE, the percentage of the difference between computed and experimental values with respect to the experimental one) is the one obtained for the structure I. It should be noted that all computational models which account for the dispersion predict structure I with a good agreement to experiment (4%) while the standard B3LYP functional gives a MAE as large as 16.2%. The fact that the B3LYP functional is not able to correctly predict a stacking intermolecular structure can be clearly understood having in mind that the standard DFT approaches do not describe properly the dispersion interaction. The relatively large discrepancy (3.7%) found for the structure resulting from simple MP2 calculations should be attributed to the BSSE, in a similar manner as for the anisole-NH_3 complex.[10,12] Indeed the MP2 counterpoise-corrected ($MP2_{CP}$) structure agrees well (1.4%) with experiment. For the excited state accuracy of computed rotational constants has been evaluated solely by a comparison with experimental data. First, we want to point out that the geometry optimization performed by a standard TD-B3LYP model starting from ground state structure I led to a T-shaped structure of the complex, not consistent with experimental findings. Then, considering dispersion-corrected TD-DFT models (listed in Table 4), similarly to the ground state, rotational constants computed for structure I deviate less from

TABLE 4: Rotational Constants (in MHz) for Structures I−III of Anisole Dimer in Its First Excited Electronic State, Computed by TD-DFT with B3LYP-D, LC-ωPBE, and M05-2X Functionals and 6-61+G(d,p) Basis Set[a]

		TD-B3LYP-D	TD-LC-ωPBE	TD-M05-2X
I	A	723.62	877.48	856.77
	B	594.20	400.01	400.39
	C	433.72	339.12	337.61
	MAE (%)	31.1	2.7	1.7
II	A		854.13	845.08
	B		367.34	361.48
	C		343.58	343.14
	MAE (%)		4.3	4.4
III	A		796.25	776.07
	B		392.14	390.32
	C		344.20	343.74
	MAE (%)		3.6	3.9

[a] The mean absolute error MAE (%) to the observed values is also reported.

experimental data, in particular a small MAE (about 1.7%) is achieved for the structure optimized at the TD-M05-2X level. It can be noted that, contrary to the ground state results, the TD-B3LYP-D structure differs strongly from the ones computed at the TD-LC-ωPBE and TD-M05-2X levels. This should be attributed to the parametrization of dispersion correction which has been performed for the ground state and does not take properly into account changes of electron density upon excitation. A similar, albeit less pronounced effect has been observed for anisole−water[9,12] and anisole−ammonia[10,12] complexes. As immediately evident, results discussed so far suggest also that the experimentally observed complex is related to the structure I. Moreover, considering the accuracy of DFT models, we shall conclude that M05-2X has yielded results with the best agreement to the computational reference data and to experi-

TABLE 5: Selected Intermolecular Parameters for Structures I−III Computed at M05-2X/6-31+G(d,p) and TD-M05-2X/6-31+G(d,p) Levels, for Ground and Excited States, Respectively[b]

		S_0[a]	S_1
I	O7H29/O23H13	3.4315	3.4170/3.3480
	O7C22/O23C6	3.4538	3.3807/3.3665
	C6C24/C8C22	3.5822	3.5570/3.5731
	C1C17	3.8631	3.7234
	O7O23	4.4979	4.3970
	O7H29C22/O23H13C6	82.14	78.95/81.72
	C8O7O23/C24O23O7	84.60	86.73/86.62
	C6O23C17/C22O7C1	64.20	86.08/85.80
	C6C24O23/C22C8O7	73.31	70.71/70.66
	C1O7O23C17	180.00	−177.74
II	O7C17/O23C1	3.5113	3.8036/3.9264
	C1C17/C2C22	3.6416	3.8890/3.2116
	C6C24/C8C18	3.5596	3.6991/3.7693
	O7O23	3.6294	3.9302
	O7C17O23/O23C1O7	83.99	85.22/80.41
	O7C17C18/O23C1C2	85.71	100.27/94.21
	C8O7C17/C24O23C1	82.89	73.19/69.53
	C1O7O23C17	−116.14	−98.76
III	O7O23	3.642	3.853
	O7C17	4.484	3.590
	O23C1	3.494	4.333
	C1C17	4.106	3.928
	C2C22	5.269	3.834
	C6C17	4.166	4.356
	C8C17	3.412	3.573
	O7O23C17	120.25	68.71
	O7C1O23	85.19	65.63
	O23C6C1	87.16	49.94
	C1O7O23C17	−57.41	−70.31

[a] For structures I and II in the ground state, because of the existing symmetry, the parameters reported in the same line have equal values. [b] Distances in angstroms and angles in degrees.

TABLE 6: Rotational constants (in MHz) of the ground and excited state structures I−III of $(C_6H_5O-CH_3)_2$, $(C_6H_5O-CH_3)$-$(C_6H_5O$-$CD_3)$ and $(C_6H_5O$-$CD_3)_2$ complexes, computed at the M05-2X/6-31+G(d,p) and TD-M05-2X/6-31+G(d,p) levels, respectively. The mean absolute error (%) to the observed values is also reported

		CH_3-CH_3	CH_3-CD_3	CD_3-CD_3	CD_3-CH_3 [a])
			S_0		
I	A	856.95	823.53	791.93	
	B	389.44	387.72	386.10	
	C	325.73	321.26	316.72	
	MAE (%)	0.7	0.8	1.1	
II	A	883.11	848.96	816.65	
	B	374.55	373.67	372.76	
	C	343.66	338.22	332.82	
	MAE (%)	4.9	4.8	4.4	
III	A	814.81	777.97	754.19	788.99
	B	363.22	360.72	355.50	357.98
	C	313.07	307.23	306.78	312.58
	MAE (%)	4.6	4.9	4.3	4.2
			S_1		
I	A	856.77	823.69	792.34	823.60
	B	400.39	398.54	396.67	398.43
	C	337.61	332.72	327.80	332.76
	MAE (%)	1.7	1.8	2.3	1.8
II	A	845.08	812.56	782.98	813.77
	B	361.48	360.86	359.14	359.85
	C	343.14	337.76	333.45	338.73
	MAE (%)	4.4	4.4	4.6	4.6
III	A	776.07	740.54	716.00	749.59
	B	390.32	388.43	382.17	383.91
	C	343.74	336.75	335.74	342.83
	MAE (%)	3.9	3.9	4.4	4.6

[a] When the structure is non symmetric, i.e. in all cases in the S_1 state and structure III in S_0, the interchange between CH_3 and CD_3 units leads to slightly different results.

ment; thus this model has been chosen for further studies. According to findings from this and earlier works,[9,10,12] the M05-2X functional can be recommended for computations of the ground and excited state equilibrium structure of complexes governed by dispersion interaction.

Equilibrium Structure and Properties of the Anisole Dimer. In order to better identify the structure of the anisole dimer, further investigation has been performed by comparison between experimental and computational studies. Ground state structures I−III correspond to complexes whose moieties have their aromatic rings placed in parallel planes, as predicted by the analysis of the experimental results. Some of their geometrical parameters computed at the M052X/6-31+G(d,p) level are listed in Table 5. For structures I and II methyl groups are placed approximately above the center of the aromatic ring of the other moiety, while structure III does not show such $CH_3-\pi$ interaction. Concerning structures I and II, the former is centrosymmetric while the latter can be described by same-side positions of methoxy substituents. As shown in Table 2 all these structures are of very similar stability; thus a more detailed analysis is necessary to associate one of them to the experimentally observed band. On the whole, comparison of the ground and excited state rotational constants (discussed in previous section) consistently shows the best agreement for structure I. It should be also noted that electronic excitation leads to lowering of symmetry of all complexes. In particular, structures II and III show a large overall deviation form their ground state counterparts and do not preserve parallel positions of the anisole molecules. Additional evidence on the equilibrium structure of anisole dimer can be obtained by the analysis of rotational constants for isotopically substituted species: the ground and excited state results computed at M05-2X/6-31+G(d,p) and TD-M05-2X/6-31+G(d,p) levels, respectively, are compared to the experimental data in Table 6. It is proven that for all combination of complexes formed between $C_6H_5O-CD_3$ and $C_6H_5O-CH_3$, the rotational constants computed for structure I agree best with their experimental counterparts, with MAE of about 1% and 2%, for the ground and excited state, respectively. Summarizing, the rotational constants of structure I show the best agreement ($\leq$2%) with experimental results for both ground and excited states and for all studied isotopic substitutions.

We shall further analyze results related to the REMPI spectrum, which provides additional insights to the structure of the complex along with information on the intermolecular interaction in anisole dimer. Computational results listed in Table 7 show a red shift of the electronic band origin (with respect to the anisole monomer) for all parallel structures; this effect is associated with larger binding energy in the excited state and results obtained for structure I show the best agreement with experiment. It should be noted that such an agreement can be only related to the change in interaction energy upon electronic excitation and does not give account to the absolute value of binding energy. The evaluation of the binding energy itself is quite difficult. Comparison of the M05-2X results with the ground state SAPT computations (described below) for anisole dimer and the previous results on anisole$-NH_3$ and anisole$-H_2O$, carried out both in the ground and in the excited state using DFT approach and coupled cluster theory, suggests

TABLE 7: Energetic Properties for Structures I−III of Anisole Dimer: Interaction Energies (in kJ/mol), $S_1 \leftarrow S_0$ Transitions (in cm^{-1}), and Their Shift Relative to Anisole Monomer (in cm^{-1})[c]

	I	II	III
	$\Delta E(S_0)$		
6-31+G(d,p)	−26.9	−25.2	−24.0
+BSSE	−23.0	−21.4	−20.2
+ZPVE	−18.6	−17.9	−17.4
aug-cc-pVTZ	−24.1	−23.3	−21.3
+BSSE	−22.1	−21.3	−19.3
+ZPVE[a]	−17.7	−17.8	−16.5
	$\Delta E(S_1)$		
6-31+G(d,p)	−33.4	−32.5	−33.6
+BSSE	−28.4	−27.6	−28.6
+ZPVE[a]	−22.2	−22.9	−23.3
aug-cc-pVTZ	−29.9	−29.1	−30.2
+BSSE	−27.8	−27.2	−28.3
+ZPVE[a]	−21.6	−22.6	−23.0
	$S_1 \leftarrow S_0$ Transition		
631+G(d,p)[a]	40328	40209	40137
aug-c-pVTZ[a]	40300	40244	40103
	Shift of $S_1 \leftarrow S_0$ Transition with Respect to Monomer		
631+G(d,p)	−546	−610	−803
+BSSE	−450	−550	−751
+ZPVE	−299	−454	−534
Aug-cc-pVTZ[a,b]	−325	−396	−540

[a] Corrected for ZPVE from harmonic frequency computations at M05-2X or TD-M052X levels with 6-31+G(d,p) basis set. [b] BSSE and ZPVE corrected. [c] Computations performed at M05-2X and TD-M05-2X levels for the ground and excited states, respectively, with 6-31+G(d,p) and aug-cc-pVTZ basis sets. Values corrected for basis set superposition error and zero-point vibrational energy are also reported.

that the interaction energies reported in Table 7 could be slightly overestimated. However, considering ΔE of about 18 and 22 kJ mol^{-1}, for the ground and excited states, respectively, as the upper limits; we can conclude that the anisole dimer is relatively weakly bound. It should be also noted that, based on the ground and excited electronic state relative stability of all parallel geometries of anisole dimer, we cannot exclude the possibility of structures II and III formation in a molecular beam condition. Moreover, even if for both of them computations predict red shifts larger (from 65 to 260 cm^{-1}) than that for structure I, the corresponding bands should be observed in the region of frequencies experimentally studied. This is even more likely given that the red shift computed for structure I overestimates by about 100 cm^{-1} the experimentally observed value (217 cm^{-1}). However, there are several possible explanations why only structure I has been observed in the current experiment. First, considering overall overestimation of energy of electronic transition origin computed by TD-DFT/DFT methods, it cannot be completely excluded that bands corresponding to the structures II and III can be found extending search further below 35710 cm^{-1} (the red limit in our experiments). Next, if anisole dimers with structure II or III exist in our molecular beam, possibly they cannot be observed because of their large changes of geometry upon electronic excitation (Table 5) which in turn cause smaller Franck−Condon factors. The latter hypothesis can be supported by the calculation of the Franck−Condon activity[48] for the origin band of the electronic transition relative to the different dimer structures, almost negligible for structures II−III and strong for structure I.

In summary, it should be concluded that extensive analysis of rotational constants confirms that band origin at 36167 cm^{-1} is related to the structure in which the two anisole molecules

TABLE 8: Components of Interaction Energies (in kJ mol^{-1}) Calculated by SAPT Theory with 6-31+G(d,p) Basis Set for Structures I−III of Anisole Dimer

	I	II	III
$E_{pol}^{(1)}$	−25.3	−21.8	−24.5
$E_{exch}^{(1)}$	45.5	41.6	38.6
$E_{ind}^{(2)}$	−19.1	−16.0	−17.5
$E_{ind\text{-}exch}^{(2)}$	16.9	13.6	15.6
$E_{disp}^{(2)}$	−37.0	−35.3	−31.4
$E_{disp\text{-}exch}^{(2)}$	5.5	5.0	4.6
E_{tot}	−13.5	−13.0	−14.6

are positioned in a parallel, centrosymmetric configuration for $(C_6H_5O-CH_3)_2$, and similarly for the other isotopically substituted complexes. The stacked arrangement of the dimer and the failure of standard B3LYP computations suggest that binding energy is dominated by the dispersion interaction. A deeper insight can be provided by an analysis of interaction energy computed for the ground state by symmetry-adapted intermolecular perturbation theory (SAPT). Table 8 lists the first- and second-order terms of interaction energy: electrostatic $E_{pol}^{(1)}$, induction $E_{ind}^{(2)}$, and dispersion $E_{disp}^{(2)}$ and their repulsive exchange counterparts $E_{exch}^{(1)}$, $E_{exch\text{-}ind}^{(2)}$, and $E_{exch\text{-}disp}^{(2)}$ obtained from the SAPT calculations.[45] For the experimentally observed structure I dispersion term is dominant and responsible for almost half of the attractive interaction. Moreover, the induction component is almost entirely quenched by its exchange counterpart; thus it can be concluded that dispersion is indeed the term that stabilizes the equilibrium structure of anisole dimer.

Conclusions

Our combined experimental and computational study has provided detailed evidence that a molecular cluster, the anisole dimer, in the gas phase is stabilized by the stacking interaction. This has been confirmed by the derived equilibrium structure, with two anisole moieties placed on parallel planes and by the analysis of interaction energy, dominated by the dispersion term. Computational studies have shown that anisole dimer is relatively weakly bound but the interaction energy is slightly larger in the excited state. The latter statement has been confirmed by the red shift of the $S_1 \leftarrow S_0$ electronic transition origin with respect to the isolated molecule. The lack of experimental evidence of the other possible dimer structures of similar stability, predicted by the computations, could be most likely attributed to the very low Franck−Condon factors for the $S_1 \leftarrow S_0$ electronic transition, given the very similar predicted stabilization energies. The experimental observation of stacked anisole dimer paves the route toward studies of possible evidence of excitonic splitting or, in other terms, to investigate if the π-electron systems of the two moieties communicate. For this purpose it is planned to extend the study to complexes with isotopic substitutions placed on the aromatic ring of anisole molecules in order to find a way to disentangle the two aromatic systems. The next step should be the search for another example of dimer in the gas phase in which the dispersion interaction could be attributed exclusively to the dispersion forces acting between the two π-electron systems.

Acknowledgment. Dr. M. Pavone is acknowledged for implementing of the DFT-D approach into the locally modified version of Gaussian package. This work was supported by Italian MIUR and by EU (under Contract No. RII3-CT-2003-506350). The large scale computer facilities of the VILLAGE network (http://village.unina.it) are kindly acknowledged. CINECA and

the Wroclaw Centre for Networking and Supercomputing are acknowledged for access to the MOLPRO code and related computer time.

References and Notes

(1) Meyer, E. A.; Castellano, R. K.; Diederich, F. *Angew Chem., Int. Ed.* **2003**, *42*, 1210–1250, and references therein.
(2) De Vries, M. S.; Hobza, P *Annu. Rev. Phys. Chem.* **2007**, *58*, 585–612.
(3) Kang, C.; Pratt, D. W.; Schäfer, M. *J. Phys. Chem. A* **2005**, *109*, 767–772.
(4) Schmitt, M.; Böhm, M.; Ratzer, C.; Krügler, D.; Kleinermanns, K.; Kalkman, I.; Berden, G.; Meerts, W. L. *ChemPhysChem* **2006**, *7*, 1241–1249.
(5) Vu, C.; Kalkman, I.; Meerts, W. L.; Svarstov, Y. N.; Jacoby, C.; Schmitt, M. *J. Chem. Phys.* **2008**, *128*, 214311.
(6) Kalkman, I.; Vu, C.; Schmitt, M.; Meerts, W. L. *ChemPhysChem* **2008**, *9*, 1788–1797.
(7) Roscioli, J. R.; Pratt, D. W. *Proc. Natl. Acad. Sci. U.S.A.* **2003**, *100*, 13752–13754.
(8) Becucci, M.; Pietraperzia, G.; Pasquini, M.; Piani, G.; Zoppi, A.; Chelli, R.; Castellucci, E.; Demtroeder, W. *J. Chem. Phys.* **2004**, *120*, 5601–5607.
(9) Pasquini, M.; Schiccheri, N.; Piani, G.; Pietraperzia, G.; Becucci, M.; Biczysko, M.; Pavone, M.; Barone, V. *J. Phys. Chem. A* **2007**, *111*, 12363–12371.
(10) Biczysko, M.; Piani, G.; Pasquini, M.; Schiccheri, N.; Pietraperzia, G.; Becucci, M.; Pavone, M.; Barone, V. *J. Chem. Phys.* **2007**, *127*, 144303.
(11) Janowski, T.; Pulay, P. *Chem. Phys. Lett.* **2007**, *447*, 27–32.
(12) Barone, V.; Biczysko, M.; Pavone, M. *Chem. Phys.* **2008**, *346*, 247–256.
(13) Grimme, S. *J. Comput. Chem.* **2006**, *27*, 1787–1799.
(14) Pavone, M.; Rega, N.; Barone, V. *Chem. Phys. Lett.* **2008**, *452*, 333–339.
(15) Zhao, Y.; Schults, N. E.; Truhlar, D. G. *J. Chem. Theory Comput.* **2006**, *2*, 364–382.
(16) Jacquemin, D.; Perpète, E.; Scalmani, G.; Frisch, M. J.; Kobayashi, R.; Adamo, C. *J. Chem. Phys.* **2007**, *126*, 144105.
(17) Arunan, E.; Gutawsky, H. S. *J. Chem. Phys.* **1993**, *98*, 4294–4296.
(18) Podeszwa, R; Bukowski, R; Szalewicz, K *J. Phys. Chem. A* **2006**, *110*, 10345–10354.
(19) Berden, G.; Meerts, W. L.; Schmitt, M.; Kleinermanns, K. *J. Chem. Phys.* **1996**, *104*, 972–982.
(20) Schmitt, M.; Ratzer, C.; Meerts, W. L. *J. Chem. Phys.* **2004**, *120*, 2752–2758.
(21) Piani, G.; Pasquini, M.; Pietraperzia, G.; Becucci, M.; Armentano, A.; Castellucci, E. *Chem. Phys. Lett.* **2007**, *434*, 25–30.
(22) Giuliano, B. M.; Caminati, W. *Angew. Chem., Int. Ed.* **2005**, *44*, 603–606.
(23) Gervasio, F. L.; Chelli, R.; Procacci, P.; Schettino, V. *Proteins* **2002**, *48*, 117–125.
(24) Chelli, R.; Gervasio, F. L.; Procacci, P.; Schettino, V. *J. Am. Chem. Soc.* **2002**, *124*, 6133–6143.
(25) Gervasio, F. L.; Chelli, R.; Procacci, P.; Schettino, V. *J. Phys. Chem. A* **2002**, *106*, 2945–2948.
(26) Tarakeshwar, P.; Kim, K. S.; Brutschy, B *J. Chem. Phys.* **1999**, *110*, 8501–8512.
(27) Kerstel, E. R. Th.; Becucci, M.; Pietraperzia, G.; Castellucci, E. *Chem. Phys.* **1995**, *199*, 263–273.
(28) Pasquini, M.; Piani, G.; Pietraperzia, G.; Demtroeder, W.; Giuntini, M.; Becucci, M. *Rev. Sci. Instrum.* **2005**, *76*, 113105.
(29) Onda, M.; Tonda, A.; Mori, S.; Yamaguchi, I. *J. Mol. Struct.* **1986**, *147*, 47.
(30) Kratochvil, M.; Sponer, J.; Hobza, P. *J. Am. Chem. Soc.* **2000**, *122*, 3495.
(31) Ryjek, F.; Kratochvil, M.; Hobza, P. *Chem. Phys. Lett.* **1999**, *313*, 393–398.
(32) Kratochvil, M.; Engkvist, O.; Jungwirth, P.; Hobza, P. *Phys. Chem. Chem. Phys.* **2000**, *2*, 2419–2424.
(33) Kratochvil, M.; Engkvist, O.; Sponer, J.; Jungwirth, P.; Hobza, P. *J. Phys. Chem. A* **1998**, *102*, 6921–6926.
(34) Ryjaek, F.; Engkvist, O.; Vacek, J.; Kratochvil, M.; Hobza, P. *J. Phys. Chem. A* **2001**, *105*, 1197–1202.
(35) Gervasio, F. L.; Procacci, P.; Cardini, G.; Guarna, A.; Giolitti, A.; Schettino, V. *J. Phys. Chem. B* **2000**, *104*, 1108–1114.
(36) Cornell, W. D.; Cieplak, P.; Bayly, C. I.; Gould, I. R; Merz, K: M:; Ferguson, D. M:; Spellmeyer, D. C.; Fox, T.; Caldwell, J. W.; Kollman, P.A. *J. Am. Chem. Soc.* **1995**, *117*, 5179–5197.
(37) Moeller, C.; Plesset, M. S. *Phys. Rev.* **1934**, *46*, 618–622.
(38) Simon, S.; Duran, M.; Dannenberg, J. *J. Chem. Phys.* **1996**, *105*, 11024–11031.
(39) Boys, S. F.; Bernardi, F. *Mol. Phys.* **1970**, *19*, 553–566.
(40) Scalmani, G.; Frish, M. J.; Mennucci, B.; Tomasi, J.; Cammi, R.; Barone, V. *J. Chem. Phys.* **2006**, *124*, 094107.
(41) Becke, D. *J. Chem. Phys.* **1993**, *98*, 5648–5652.
(42) Frisch, M. J.; Trucks, G. W.; Schlegel, H. B.; Scuseria, G. E.; Robb, M. A.; Cheeseman, J. R.; Montgomery, J. A., Jr.; Vreven, T.; Kudin, K. N.; Burant, J. C.; Millam, J. M.; Iyengar, S. S.; Tomasi, J.; Barone, V.; Mennucci, B.; Cossi, M.; Scalmani, G.; Rega, N.; Petersson, G. A.; Nakatsuji, H.; Hada, M.; Ehara, M.; Toyota, K.; Fukuda, R.; Hasegawa, J.; Ishida, M.; Nakajima, T.; Honda, Y.; Kitao, O.; Nakai, H.; Klene, M.; Li, X.; Knox, J. E.; Hratchian, H. P.; Cross, J. B.; Bakken, V.; Adamo, C.; Jaramillo, J.; Gomperts, R.; Stratmann, R. E.; Yazyev, O.; Austin, A. J.; Cammi, R.; Pomelli, C.; Ochterski, J. W.; Ayala, P. Y.; Morokuma, K.; Voth, G. A.; Salvador, P.; Dannenberg, J. J. ; Zakrzewski, V. G.; Dapprich, S.; Daniels, A. D.; Strain, M. C.; Farkas, O.; Malick, D. K.; Rabuck, A. D.; Raghavachari, K.; Foresman, J. B.; Ortiz, J. V.; Cui, Q.; Baboul, A. G.; Clifford, S.; Cioslowski, J.; Stefanov, B. B.; Liu, G.; Liashenko, A.; Piskorz, P.; Komaromi, I.; Martin, R. L.; Fox, D. J.; Keith, T.; Al-Laham, M. A.; Peng, C. Y.; Nanayakkara, A.; Challacombe, M.; Gill, P. M. W.; Johnson, B.; Chen, W.; Wong, M. W.; Gonzalez, C.; Pople, J. A. *Gaussian Development Version, revision G.01*; Gaussian, Inc.: Wallingford, CT, 2006.
(43) Hampel, C.; Peterson, K.; Werner, H.-J. *Chem. Phys. Lett.* **1992**, *190*, 1–12.
(44) Dunning, T. H., Jr. *J. Chem. Phys.* **1989**, *90*, 1007–1023.
(45) Jeziorski, B.; Moszynski, R.; Szalewicz, K. *Chem. Rev.* **1994**, *94*, 1887–1930.
(46) Werner, H.-J.; Knowles, P. J.; Lindh, R.; Manby, F. R.; Schütz, M.; Celani, P.; Korona, T.; Rauhut, G.; Amos, R. D.; Bernhardsson, A.; Berning, A.; Cooper, D. L.; Deegan, M. J. O.; Dobbyn, A. J.; Eckert, F.; Hampel, C.; Hetzer, G.; Lloyd, A. W.; McNicholas, S. J.; Meyer, W.; Mura, M. E.; Nicklass, A.; Palmieri, P.; Pitzer, R.; Schumann, U.; Stoll, H.; Stone, A. J.; Tarroni, R.; Thorsteinsson, T. *MOLPRO, version 2006.1*, http://www.molpro.net.
(47) Plusquellic, D. F. http://physics.nist.gov/jb95; NIST: Gaithersburg, MD, 2003.
(48) Barone, V.; Bloino, J.; Biczysko, M.; Santoro, F. *J. Chem. Theory Comput.* **2009**, *5*, 540–554.

JP903236Z